ARTICLE IN PRESS

ELSEVIER

Journal of Wind Engineering
and Industrial Aerodynamics ▮ (▮▮▮▮) ▮▮▮–▮▮▮

JOURNAL OF wind engineering AND industrial aerodynamics

www.elsevier.com/locate/jweia

Thin water film around a cable subject to wind

C. Lemaitre, P. Hémon*, E. de Langre

Department of Mechanics, LadHyX, CNRS-Ecole Polytechnique, 91128 Palaiseau, France

Abstract

Cables of cable-stayed bridges can experience rain–wind-induced vibrations (RWIV). This instability involves lower frequencies and higher amplitudes than classical vortex-induced vibrations. Furthermore, RWIV is restricted to a certain range of wind velocities, unlike linear 1 dof galloping. When flowing along the cables, the water gathers near the separation points to form one or two rivulets. Former studies which have described the coupling between the rivulets' motion and the cable motion assume the existence of at least one rivulet. In this paper, we address the conditions for the formation of the rivulets. A two-dimensional model is developed within the lubrication theory, describing the evolution of a thin film subjected to gravity, surface tension, wind and motion of the cylinder. Numerical simulations show the appearance of the rivulets that are reputedly responsible for the instability. The position at which the rivulets appear is found to vary with the wind speed and the predictions of the model are in good agreement with new experimental data.

Keywords: Rain–wind-induced vibrations; Cylinder; Rivulet; Film dynamics; Lubrication theory

1. Introduction

On cable-stayed bridges, inclined cables connect the pylons to the deck, Fig. 1. The cables can experience vibrations which are due to the presence of both rain and wind (rain–wind-induced vibrations, RWIV). First reported by Hikami and Shiraishi (1988), this particular type of instability happens under conditions of moderate rain and rather low wind speed, typically 10 m/s, and vibrations cease when the rain stops. Unlike the instabilities due solely to wind, RWIV are not fully understood. Observations in full-scale as well as experiments conducted in wind tunnels show that RWIV occurs only in cables

*Corresponding author. Tel.: +33 1 69 33 39 33; fax: +33 1 69 33 30 30.
E-mail address: pascal.hemon@ladhyx.polytechnique.fr (P. Hémon).

0167-6105/$ - see front matter © 2007 Elsevier Ltd. All rights reserved.
doi:10.1016/j.jweia.2007.02.007

Please cite this article as: Lemaitre, C., et al., Thin water film around a cable subject to wind, J. Wind Eng. Ind. Aerodyn. (2007), doi:10.1016/j.jweia.2007.02.007

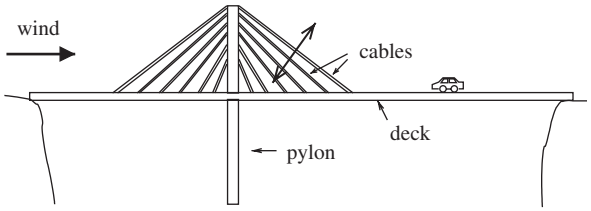

Fig. 1. Cable-stayed bridge. Only cables declining in the wind direction undergo RWIV.

declining in the direction of the wind. The vibrations are generally cross-wind (Hikami and Shiraishi, 1988). The amplitudes of such vibrations are higher, and the frequencies lower, than those of vortex-induced vibrations (Hikami and Shiraishi, 1988). Furthermore, this is a velocity-restricted phenomenon, unlike the linear one-degree-of-freedom galloping of Den Hartog (1985), for which there is no maximum wind speed.

In unstable cases, the water flows around the cable and one to two rivulets form near the separation points of the air flow around the dry cylinder (Bosdogianni and Olivari, 1996). The two rivulets oscillate circumferentially, at the same frequency as the cable motion, (Hikami and Shiraishi, 1988). Some sine waves travel along the upper rivulet, whereas the bottom rivulet stays rectilinear (Wang et al., 2005). Authors agree that the presence of the upper rivulet is required for the instability to take place (Matsumoto et al., 1995; Bosdogianni and Olivari, 1996). It is unclear, however, whether the circumferential motion of the upper rivulet is necessary or not. Experiments by Verwiebe and Ruscheweyh (1998) and Flamand (1995) tend to show that an artificial rivulet fixed on the cylinder, exposed to a RWIV-like wind, does not provoke instability. On the contrary, Bosdogianni and Olivari (1996) and Matsumoto et al. (1995) observe vibrations of the cable in similar experiments.

RWIV causes fatigue and necessitates earlier replacement of the cables. Countermeasures to avoid this phenomenon that are based on the disorganization of the rivulets have been studied. Flamand (1995) and more recently Gu and Du (2005) have tested several solutions such as a wire spiralling around the cable.

Some models intended to describe the coupling between the upper rivulet and the cable motion have been developed. Yamaguchi (1990) presented a galloping model with two-degrees-of-freedom, which has been extended more recently by Peil and Nahrath (2003) and Peil et al. (2003) to more degrees-of-freedom.

These models assume the existence of at least the upper rivulet. In this article, the conditions for the appearance of the rivulets are investigated. A new model is presented in Section 2 that describes the evolution of a thin water film around a moving cable subject to wind. Numerical results from this model are discussed in Section 3. In Section 4, the position of the rivulets predicted by the model is compared to data from new experiments.

The details for the derivation of the model may be found in Lemaitre (2006). Some more experiments and a simple criterion for determining the existence and the position of the rivulets are presented in Lemaitre et al. (2006).

2. Model

This section presents a new two-dimensional model based on lubrication theory. The model describes the behaviour of a thin water film in a cylindrical configuration, evolving

Please cite this article as: Lemaitre, C., et al., Thin water film around a cable subject to wind, J. Wind Eng. Ind. Aerodyn. (2007), doi:10.1016/j.jweia.2007.02.007

under the effect of gravity, surface tension, wind and motion of the support. Reisfeld and Bankoff (1992) derived the equations for a thin film surrounding a cylinder, subject to gravity and surface tension. Following a similar approach we modelled the actions of wind and cable motion on the film, by considering them as an external forcing.

2.1. Geometry and notations

A thin film of thickness $h(\theta)$ is considered, surrounding a horizontal cylinder of radius R (Fig. 2). The film is assumed to be continuous: there is no dewetting and the quantity of matter is constant (no drop break-off). It has a characteristic thickness h_0. It is subject to gravity $\mathbf{g} = -g\mathbf{e}_y$ and to a homogeneous surface tension, γ, independent of θ. If an inclined cylinder were considered instead of a horizontal one, the effective gravity would be lower. The wind blows from the left with a horizontal upstream velocity $\mathbf{v}_{g\infty} = v_{g\infty}\mathbf{e}_x$ that produces pressure and friction coefficients $C_p(\theta)$ and $C_f(\theta)$, respectively, at each point on the film surface. As the rain–wind-induced vibrations are mostly transverse to the wind direction, the cable may undergo a vertical motion. Its displacement, $\mathbf{y} = y\mathbf{e}_y$, has a characteristic amplitude y_0 and its evolution in time, with a characteristic time T_y, is described by a function f, $y(t) = y_0 f(t/T_y)$, which is assumed to be twice differentiable. The function f might be a sine-function; the time T_y would then be its period. The acceleration of the cable produces an added gravity that depends on time,

$$\mathbf{g}_a = -\ddot{y}\mathbf{e}_y = -\frac{y_0}{T_y^2} f''\left(\frac{t}{T_y}\right)\mathbf{e}_y. \tag{1}$$

2.2. Navier–Stokes and boundary conditions

The Navier–Stokes equations are written for the water film,

$$\begin{cases} \rho\dfrac{D\mathbf{v}}{Dt} = \rho(\mathbf{g} + \mathbf{g}_a) - \boldsymbol{\nabla} p + \mu\Delta\mathbf{v}, \\ \boldsymbol{\nabla}.\mathbf{v} = 0, \end{cases} \tag{2}$$

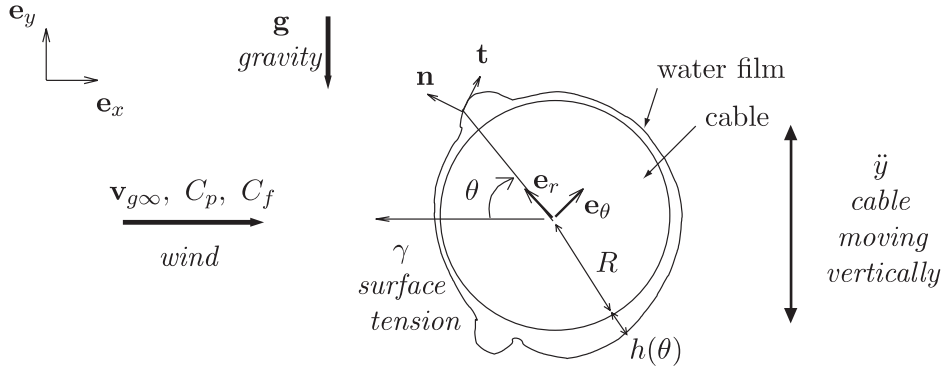

Fig. 2. Water film around a cable subject to gravity, surface tension and swept by wind.

Please cite this article as: Lemaitre, C., et al., Thin water film around a cable subject to wind, J. Wind Eng. Ind. Aerodyn. (2007), doi:10.1016/j.jweia.2007.02.007

where $\mathbf{v}$ is the velocity field in the water film, ρ is the water density, p is the pressure in the film and μ is the dynamic viscosity of water. In the local frame $(\mathbf{e}_r, \mathbf{e}_\theta)$, the position of a water particle is expressed as $\mathbf{r} = r\mathbf{e}_r$ $(R \leqslant r \leqslant R + h)$ and its velocity decomposes into $\mathbf{v} = u\mathbf{e}_r + v\mathbf{e}_\theta$. The Navier–Stokes equations are written in cylindrical coordinates, see Eq. (A.1) in the Appendix A.

In the whole paper, partial differentiation in space and time will be noted ∂_θ, ∂_ξ, ∂_t and ∂_T. The order of differentiation, n, will be indicated by superscripts, ∂^n.

The associated boundary conditions are: (i) the water particles do not slip on the cable,

$$u = v = 0. \tag{3}$$

(ii) The water–air interface is a material surface that no water particle can cross. The normal velocity of a water particle on the interface is thus equal to the normal velocity of the interface,

$$u = \partial_t h + \frac{v}{r}\partial_\theta h. \tag{4}$$

(iii) The jump in the normal shear stress is balanced by the surface tension (Batchelor, 1994)

$$(\boldsymbol{\sigma}_g - \boldsymbol{\sigma})\mathbf{n} = \mathscr{K}\gamma\mathbf{n}, \quad \boldsymbol{\sigma} = -p\mathbf{I} + \mu[\boldsymbol{\nabla}\mathbf{v} + (\boldsymbol{\nabla}\mathbf{v})^{\mathrm{T}}], \quad \boldsymbol{\sigma}_g = -p_g(\theta)\mathbf{I} + \boldsymbol{\tau}_g, \tag{5}$$

where $\boldsymbol{\sigma}_g$ and $\boldsymbol{\sigma}$ are the stress tensors of the gas and the water, respectively, γ is the surface tension, $\mathbf{I}$ is the identity tensor, p_g is the air pressure at the interface and $\boldsymbol{\tau}_g$ is the viscous stress tensor of air. At each point of the water–air interface, the normal and tangential vectors read,

$$\mathbf{t} = \frac{1}{N}\left(\frac{\partial_\theta h}{r}\mathbf{e}_r + \mathbf{e}_\theta\right), \quad \mathbf{n} = \frac{1}{N}\left(\mathbf{e}_r - \frac{\partial_\theta h}{r}\mathbf{e}_\theta\right), \quad N = \left(1 + \frac{(\partial_\theta h)^2}{r^2}\right)^{1/2}. \tag{6}$$

The curvature $\mathscr{K}(\theta)$ of the free surface of the film is Ibrahim (2005)

$$\mathscr{K}(\theta) = \boldsymbol{\nabla}.\mathbf{n} = \frac{(R+h)^2 + 2(\partial_\theta h)^2 - (R+h)\partial_\theta^2 h}{[(R+h)^2 + (\partial_\theta h)^2]^{3/2}}. \tag{7}$$

The boundary conditions are thus expressed in cylindrical coordinates, which may be found in the appendix (Eq. (A.3)).

2.3. Lubrication and dimensionless equations

The assumptions of lubrication are now made: (a) the Reynolds number based on the film thickness is close to one, $Re_h = h_0 v/\nu \approx 1$; (b) the film is thin compared to the cable radius, $h_0 \ll R$; (c) the film thickness h evolves 'slowly' with θ, $\partial_\theta h \ll R$. As a consequence, the following dimensionless variables are defined for the liquid

$$U = \frac{R}{\nu}u, \quad V = \frac{h_0}{\nu}v, \quad T = \frac{\nu}{Rh_0}t,$$

$$P = \frac{h_0^3}{\rho\nu^2 R}p, \quad \xi = \frac{r-R}{h_0}, \quad H = \frac{h}{h_0}. \tag{8}$$

They are based on viscosity scales and are assumed to be of the order of one.

Please cite this article as: Lemaitre, C., et al., Thin water film around a cable subject to wind, J. Wind Eng. Ind. Aerodyn. (2007), doi:10.1016/j.jweia.2007.02.007

An external wind load is acting on the water surface. This load is nondimensionalized with the classic pressure coefficient and a normalized friction coefficient which has been divided by its maximum value,

$$C_{\mathrm{f}} = \frac{\mathbf{t}.\boldsymbol{\tau}_{\mathrm{g}}.\mathbf{n}}{(1/2)\rho_{\mathrm{g}} v_{\mathrm{g}\infty}^2}, \quad \overline{C}_{\mathrm{f}} = \frac{C_{\mathrm{f}}}{\max(C_{\mathrm{f}})}. \tag{9}$$

When writing the Navier–Stokes and the boundary condition equations in a non-dimensional form, Eqs. (A.4) and (A.5) of the appendix, the small parameter $\varepsilon = h_0/R$ and the following dimensionless numbers appear:

$$G = \frac{g h_0^3}{3\nu^2}, \quad S = \frac{\gamma h_0^4}{3\rho\nu^2 R^3}, \quad \mathscr{A} = \frac{y_0 h_0^3}{3\nu^2 T_y^2}, \quad \Omega_y = \frac{2\pi R h_0}{\nu T_y},$$

$$\mathscr{P} = \frac{\rho_{\mathrm{g}} v_{\mathrm{g}\infty}^2 h_0^3}{6\rho\nu^2 R}, \quad \mathscr{F} = \frac{\rho_{\mathrm{g}} v_{\mathrm{g}\infty}^2 h_0^2 \max(C_{\mathrm{f}})}{4\rho\nu^2}. \tag{10}$$

The numbers G, S, $\mathscr{A}$, $\mathscr{P}$ and $\mathscr{F}$ compare the actions of gravity, surface tension, cable acceleration, air pressure and air friction, respectively, to the action of water viscosity. The reduced pulsation Ω_y compares the cable motion characteristic time to the viscous time.

Only the terms of leading order in ε are retained, yielding the linearized Navier–Stokes equations

$$\begin{aligned}
&\partial_\xi P = 0,\\
&-3\left(G + \mathscr{A} f''\left(\frac{\Omega_y}{2\pi}T\right)\right)\cos\theta - \partial_\theta P + \partial_\xi^2 V = 0,\\
&\partial_\xi U + \partial_\theta V = 0
\end{aligned} \tag{11}$$

and the linearized boundary condition

$$\begin{aligned}
&U|_{\xi=0} = V|_{\xi=0} = 0,\\
&U|_{\xi=H} = \partial_T H + V|_{\xi=H}\partial_\theta H,\\
&-3\mathscr{P}C_{\mathrm{p}} + P|_{\xi=H} = 3S\left(\frac{1}{\varepsilon} - H - \partial_\theta^2 H\right),\\
&2\mathscr{F}\overline{C}_{\mathrm{f}} - (V_\xi)|_{\xi=H} = 0.
\end{aligned} \tag{12}$$

Eq. (11c) is integrated between $\xi = 0$ and $\xi = H$; the condition $U|_{\xi=0} = 0$ is then used,

$$U = -\int_{\xi=0}^{H} \partial_\theta V \,\mathrm{d}\xi. \tag{13}$$

This is injected into Eq. (12b) and condensed into

$$\partial_T H + \partial_\theta\left[\int_{\xi=0}^{H} V \,\mathrm{d}\xi\right] = 0. \tag{14}$$

The pressure in the water film P is independent of ξ (Eq. (11a)). The expression for P given by Eq. (12c) is thus valid in the whole film and is injected into Eq. (11b),

$$\partial_\xi^2 V = 3(G + \mathscr{A} f'')\cos\theta + \partial_\theta\left[3S\left(\frac{1}{\varepsilon} - H - \partial_\theta^2 H\right) + 3\mathscr{P}C_{\mathrm{p}}\right]. \tag{15}$$

Please cite this article as: Lemaitre, C., et al., Thin water film around a cable subject to wind, J. Wind Eng. Ind. Aerodyn. (2007), doi:10.1016/j.jweia.2007.02.007

This last equation is integrated twice with respect to ξ and Eqs. (12a) and (12d) are used to obtain

$$V = \tfrac{3}{2}[(G + \mathscr{A}f'')\cos\theta - S(\partial_\theta H + \partial_\theta^3 H) + \mathscr{P}\partial_\theta(C_p)](\xi^2 - 2H\xi) + 2\mathscr{F}\overline{C}_f\xi. \tag{16}$$

This expression for the azimuthal velocity is replaced in Eq. (14) and we finally obtain

$$\partial_T H + \partial_\theta\{-[G + \mathscr{A}f''(\Omega_y T/2\pi)]H^3\cos\theta + S(\partial_\theta H + \partial_\theta^3 H)H^3 - \mathscr{P}\partial_\theta(C_p)H^3 + \mathscr{F}\overline{C}_f H^2\} = 0. \tag{17}$$

This is an equation of conservation of the thickness H, with a flux g,

$$\partial_T H + \partial_\theta g = 0,$$
$$g = [-(G + \mathscr{A}f'')\cos\theta + S(\partial_\theta H + \partial_\theta^3 H) - \mathscr{P}\partial_\theta(C_p)]H^3 + \mathscr{F}\overline{C}_f H^2. \tag{18}$$

For $\mathscr{A} = 0$, $\mathscr{P} = 0$ and $\mathscr{F} = 0$, Eq. (17) is the same as that presented by Reisfeld and Bankoff (1992, Eq. (4.16)). The form of the air friction term is consistent with Eq. (2.31) of Oron et al. (1997) for a thin film on a plane.

3. Evolution of a film under a wind load

In this section, Eq. (17) is solved in the range of typical parameter for rain–wind-induced vibrations. It is assumed here that the wind load on the film is the same as the wind load that would apply around the dry cable. The values of the wind load around a dry cable are supposed to apply along the local normal and tangent vectors of the water film. The Reynolds number based on the cable diameter in RWIV conditions is

$$Re_g = \frac{2Rv_{g\infty}}{v_g} \approx 10^5, \tag{19}$$

where v_g is the air viscosity, the typical cable radius being $R = 0.1$ m and the typical wind speed $v_{g\infty} = 10$ m/s. Achenbach (1968) measured the pressure and friction distributions produced by an air flow on a smooth cylinder oriented in the cross-flow direction. His results at the same Reynolds number are used for the computations (Fig. 3).

The control parameters of Eq. (17) have been computed for experiments from the literature in Table 1, with a typical water thickness of $h_0 = 5 \times 10^{-4}$ m. It is remarkable that the pressure number $\mathscr{P}$ and the friction number $\mathscr{F}$ are of the same order of magnitude. The friction of air will consequently have a major effect on the dynamics of the film and cannot be neglected.

Eq. (17) is a partial differential equation of the fourth order that is nonlinear with nonconstant coefficients. It is thus not solvable analytically and numerical computations are needed. The computations are carried out with a pseudo-spectral method: a Fourier spectral method in space and an Adams–Bashforth scheme of the fourth order in time. Fig. 4 shows a resolution of Eq. (17) with a static cable, $\mathscr{A} = 0$ and the other parameters computed from Flamand (1995). At the initial time, the thickness of the film is constant in space, $H(0,\theta) = 1$. The resolution in space is of $N_x = 128$ points and the time step is $dT = 10^{-6}$. At the top and at the bottom of the cylinder, two water bulges form, which are the bidimensional traces of the rivulets. They are located in the neighbourhood of the

Please cite this article as: Lemaitre, C., et al., Thin water film around a cable subject to wind, J. Wind Eng. Ind. Aerodyn. (2007), doi:10.1016/j.jweia.2007.02.007

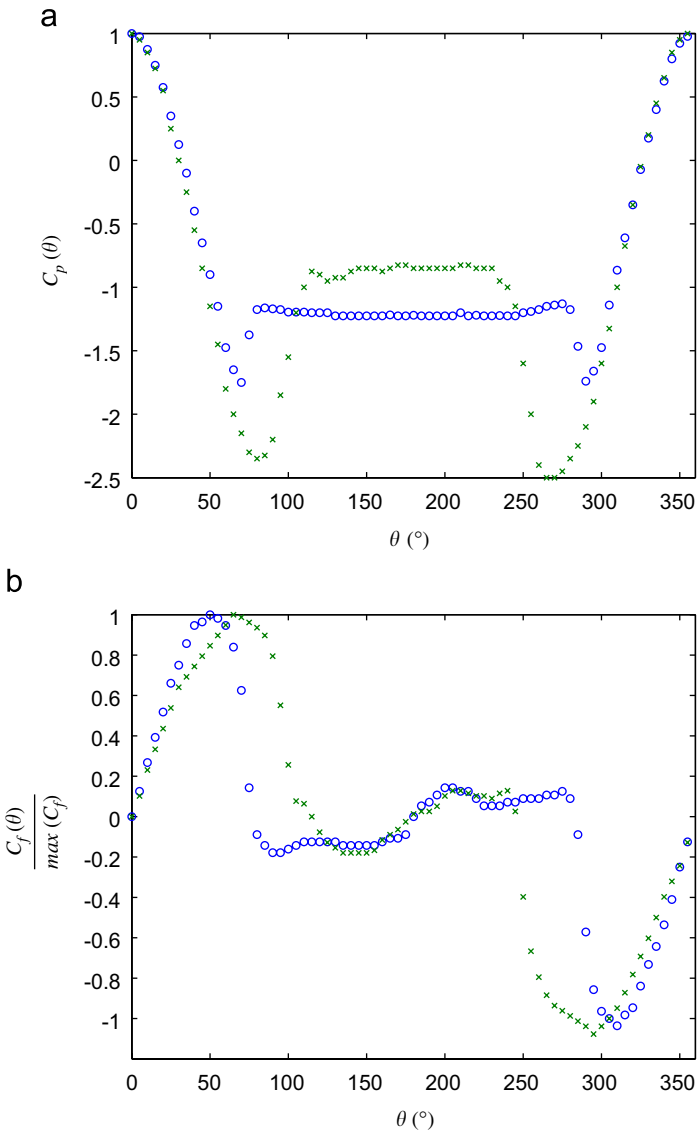

Fig. 3. Distribution of the wind load around a smooth dry cylinder at (○) $Re_g = 10^5$ and (×) $Re_g = 3.6 \times 10^6$, measured by Achenbach (1968): (a) pressure coefficients; (b) normalized friction coefficients. The maximum of the subcritical friction coefficient is $\max(C_f) = 1.7 \times 10^{-2}$ and $\max(C_f) = 4.1 \times 10^{-3}$ in the supercritical case.

separation points that would be exhibited by the air flow around the dry cylinder. The bulges' size increases until the lubrication assumptions are violated. Under the effect of gravity the bottom protuberance grows faster than the upper one. As observed by Reisfeld and Bankoff (1992), a cusp is bound to appear at $\theta = 3\pi/2$ under gravity action, but its formation is slower than the dynamics of formation of the rivulets due to wind loads.

Please cite this article as: Lemaitre, C., et al., Thin water film around a cable subject to wind, J. Wind Eng. Ind. Aerodyn. (2007), doi:10.1016/j.jweia.2007.02.007

Table 1
Parameter values for experiments from the literature

Authors	ε	G	S	$\mathscr{A}$	Ω_y	$\mathscr{P}$	$\mathscr{F}$
Hikami and Shiraishi (1988)							
Full-scale	7.1×10^{-3}	4.1×10^{2}	4.4×10^{-3}	27	4.4×10^{2}	43	1.6×10^{2}
Wind tunnel	7.1×10^{-3}	4.1×10^{2}	4.4×10^{-3}	4.6	2.2×10^{2}	43	1.6×10^{2}
Flamand (1995)	6.3×10^{-3}	4.1×10^{2}	3.0×10^{-3}	7.5	2.5×10^{2}	38	1.6×10^{2}
Matsumoto et al. (1995)	5.9×10^{-3}	4.1×10^{2}	2.5×10^{-3}	2.2	1.5×10^{2}	29	1.3×10^{2}

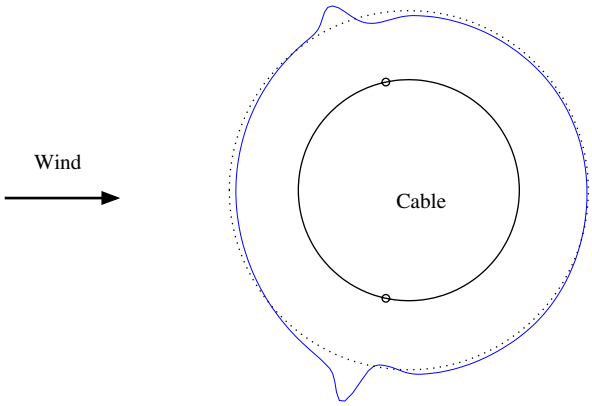

Fig. 4. Numerical solution of Eq. (17) starting from a homogeneous film, subjected to gravity, surface tension and wind. The cable radius is $R = 0.08$ m. The film thickness shown is one hundred times the actual thickness. $(\cdots)$ film at $t = 0$ s; $(-)$ film at $t = 6.9 \times 10^{-3}$ s ($T = 1.7 \times 10^{-5}$); $(\circ)$ separation points of the air flow around the dry cable.

In order to study the relative effects of friction and pressure, the two following artificial cases are considered:

(i) A film of initial constant thickness is subjected to surface tension ($S = 3.0 \times 10^{-3}$) and pressure ($\mathscr{P} = 3.8 \times 10^{1}$), the other terms of Eq. (17) being set to zero ($G = 0$, $\mathscr{A} = 0$ and $\mathscr{F} = 0$).
(ii) Another computation is done in which only the terms due to surface tension ($S = 3.0 \times 10^{-3}$) and friction ($\mathscr{F} = 1.6 \times 10^{2}$) are retained ($G = 0$, $\mathscr{A} = 0$ and $\mathscr{P} = 0$).

The same numerical parameters as above are implemented ($N_x = 128$, $\mathrm{d}T = 10^{-6}$) to give the results which are presented in Fig. 5. Both computations show the appearance and growth of two rivulets in the region of the separation points. The rivulets created by friction grow with a characteristic time similar to the time necessary to form the rivulets under pressure. Moreover, the rivulets due to pressure are located slightly upstream of the friction generated rivulets. The action of friction appears to be of same importance as the pressure action in the rivulet generation.

Please cite this article as: Lemaitre, C., et al., Thin water film around a cable subject to wind, J. Wind Eng. Ind. Aerodyn. (2007), doi:10.1016/j.jweia.2007.02.007

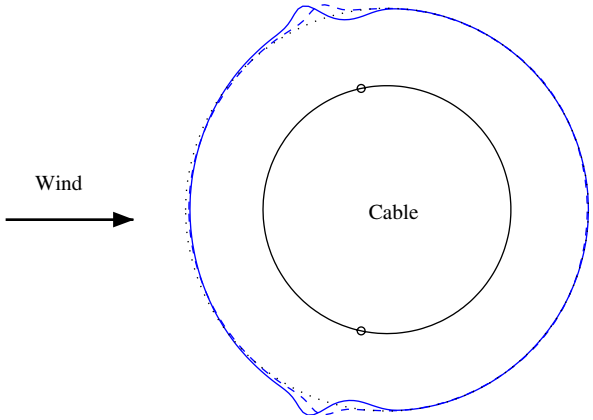

Fig. 5. Comparison of pressure and friction actions. The cable radius is $R = 0.08\,\mathrm{m}$. The films shown at $t = 6.9 \times 10^{-3}\,\mathrm{s}$ ($T = 1.7 \times 10^{-5}$) are one hundred times the actual size: (−) film evolving under pressure and surface tension only; (−−) film evolving under friction and surface tension only; (○) separation points of the air flow around the dry cable.

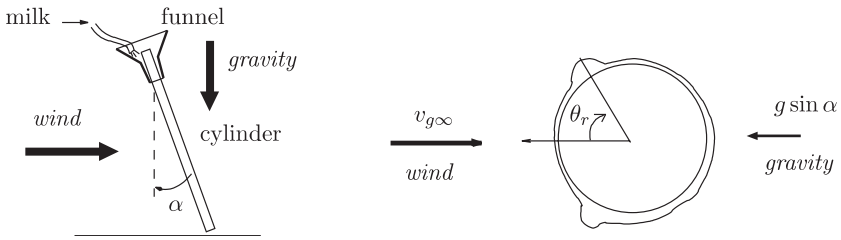

Fig. 6. Experimental setup for the study of the position at which the rivulets appear. In a wind tunnel, a cylinder is inclined in the direction of the flow. It is covered with milk that is fed from the top through a funnel: (a) side view; (b) a cylinder section.

4. Position of the rivulets

In this section, we focus on the position at which the rivulets are formed. A new experiment has been conducted in the Mechanical Engineering Department of the Hong Kong Polytechnic University. A black cylinder continuously coated with milk, which flows from a funnel reservoir, is hung in a wind tunnel. The cylinder is fixed, slightly inclined from the vertical at an angle $\alpha = 2.5^\circ$, declining without yaw in the wind direction (Fig. 6). The setup is video-recorded from the side and optically treated to access to the position of the rivulets, θ_r.

In Sections 2 and 3, the gravity was orthogonal to the wind direction. On the contrary, in the experimental configuration, the projection of the gravity on a plane normal to the cylinder axis, $g \sin \alpha$, is parallel to the projected wind direction, $v_{g\infty}$, Fig. 6(b), and our model reads

$$\partial_T H + \partial_\theta\{[-G \sin\alpha \sin\theta + S(\partial_\theta H + \partial_\theta^3 H) - \mathscr{P}\partial_\theta(C_p)]H^3 + \mathscr{F}\overline{C}_f H^2\} = 0. \tag{20}$$

Note that there is no term due to the acceleration of the cylinder, since it is static in the experiment.

Please cite this article as: Lemaitre, C., et al., Thin water film around a cable subject to wind, J. Wind Eng. Ind. Aerodyn. (2007), doi:10.1016/j.jweia.2007.02.007

The position of the thickness maxima can be computed for several wind speeds by using the numerical method presented in the previous section. The cylinder radius is $R = 7.5 \times 10^{-3}$ m and the tested wind speed ranges from $v_{g\infty} = 0$ to 10 m/s so that the Reynolds number of the air flow based on the diameter is subcritical $Re_g = 2Rv_{g\infty}/v_g = 0$–$10^4$. However, the rivulets are located close to the separation points so that transition might occur due to a rugosity effect (Szechenyi, 1975) and the flow might become supercritical. Therefore, the computations have been conducted both for subcritical and supercritical wind loads (see the pressure and friction distributions for both the cases in Fig. 3). The pressure and the friction numbers $\mathscr{P}$ and $\mathscr{F}$ are proportional to the square of the wind velocity. In Fig. 7, the position of the rivulets, θ_r is plotted as a function of $v_{g\infty}^2$.

The theoretical results are found to be in good agreement with the experiments. In the absence of air flow, a single rivulet exists at $\theta_r = 0°$. When the wind tunnel is turned on, the competition of gravity with wind pressure and friction results in the formation of one or two rivulets, whose positions depend on the wind speed. At low airspeed, only one rivulet forms at $\theta_r = 0°$; when the speed is increased, the single rivulet splits up into two symmetrical rivulets; the rivulets move leeward as the flow speed is further augmented; a maximum position $\theta_r = \theta_{max}$ is then reached. The experimental saturation angle $\theta_{max}^{exp} = 78°$ is bounded by the subcritical and supercritical values, $\theta_{max}^{sub} = 68°$ and $\theta_{max}^{sup} = 91°$, which may indicate that laminar-turbulent transition of the boundary layer occurs.

5. Conclusion

We have presented here a model that describes for the first time the evolution of a water film around a cylinder under the action of wind and cylinder motion. This model recovers

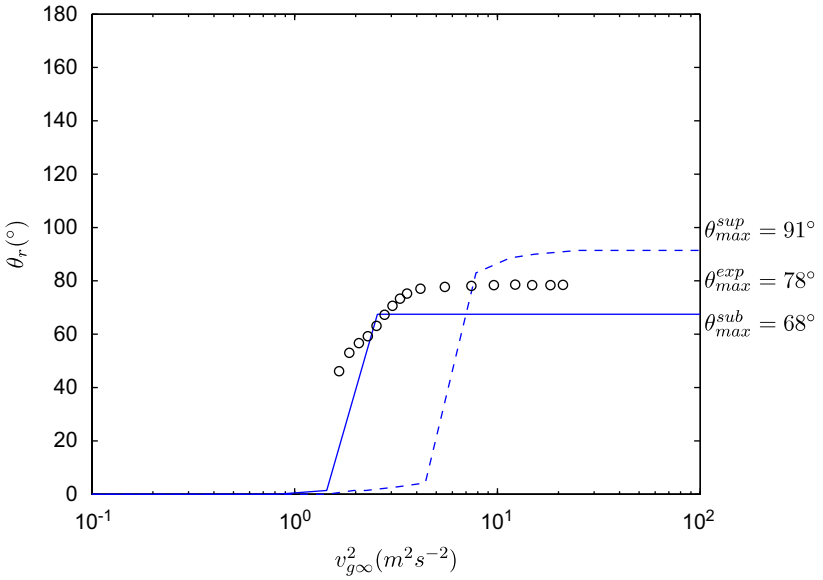

Fig. 7. Position θ_r of one rivulet as a function of the wind speed $v_{g\infty}$. A second rivulet exists at the symmetrical position $-\theta_r$. Experimental results (○). Theoretical results for subcritical coefficients (–) and for supercritical coefficients (––).

Please cite this article as: Lemaitre, C., et al., Thin water film around a cable subject to wind, J. Wind Eng. Ind. Aerodyn. (2007), doi:10.1016/j.jweia.2007.02.007

well the appearance of the two water rivulets that are claimed to be responsible for rain–wind-induced vibration of cables of cable-stayed bridges. In accordance with previous experimental observations, the rivulets form in the region of the separation points of the air flow around the dry cable under the combined effect of air pressure and friction. The friction is shown to play a significant role in the generation of the rivulets. In rain–wind-induced vibrations, the lift force is related to the position of the rivulets for which we provided here a predictive model. The angular position of the rivulets, θ_r, has been also investigated experimentally. The angle θ_r is found to be an increasing function of the wind velocity for low velocities where gravity is progressively overcome by wind action. For higher velocities however, the position is independent of the wind velocity and experimental results range between the values computed with subcritical and supercritical aerodynamic pressure data.

Acknowledgements

The authors gratefully acknowledge the kind help of J. Huang, Dr. M. Alam and Pr. Y. Zhou from Hong Kong Polytechnic University as well as the financial support of the France–Hong Kong PROCORE joint research program 07708UE on Rain–wind-Induced Vibrations of cables, which made the experiments possible.

Appendix A

In the local frame $(\mathbf{e}_r, \mathbf{e}_\theta)$ the Navier–Stokes equations (2) read,

$$\rho\left(\partial_t u + u\partial_r u + \frac{v}{r}\partial_\theta u - \frac{v^2}{r}\right) = \rho(\mathbf{g}+\mathbf{g}_a).\mathbf{e}_r - \partial_r p + \mu\left(\Delta u - \frac{2\partial_\theta v}{r^2} - \frac{u}{r^2}\right),$$

$$\rho\left(\partial_t v + u\partial_r v + \frac{v}{r}\partial_\theta v + \frac{uv}{r}\right) = \rho(\mathbf{g}+\mathbf{g}_a).\mathbf{e}_\theta - \partial_\theta p + \mu\left(\Delta v - \frac{2\partial_\theta u}{r^2} - \frac{v}{r^2}\right),$$

$$\frac{\partial_r(ru)}{r} + \frac{\partial_\theta v}{r} = 0, \tag{A.1}$$

where the operator Δ applied on a scalar s signifies

$$\Delta s = \frac{\partial_r(r\partial_r s)}{r} + \frac{\partial_\theta^2 s}{r^2}. \tag{A.2}$$

The boundary conditions on the air–water interface at $r = R + h$, Eq. (5), are also expressed in cylindrical coordinates,

$$\begin{aligned} &-p_g + p - \frac{2\mu}{N^2 r}\left\{(u+\partial_\theta v)\left[\left(\frac{\partial_\theta h}{r}\right)^2 - 1\right] - \partial_\theta h\partial_r\left(r\left(\frac{v}{r}\right) + \frac{\partial_\theta u}{r}\right)\right\} \\ &\quad = \frac{\gamma}{N^3}\left(\frac{1}{r} + 2\frac{(\partial_\theta h)^2}{r^3} - \frac{\partial_\theta^2 h}{r^2}\right), \\ &t_g - \frac{\mu}{N^2}\left\{-\frac{4\partial_\theta h}{r^2}(u+\partial_\theta v) + \left[1 - \left(\frac{\partial_\theta h}{r}\right)^2\right]\left(r\partial_r\left(\frac{v}{r}\right) + \frac{\partial_\theta u}{r}\right)\right\} = 0. \end{aligned} \tag{A.3}$$

Please cite this article as: Lemaitre, C., et al., Thin water film around a cable subject to wind, J. Wind Eng. Ind. Aerodyn. (2007), doi:10.1016/j.jweia.2007.02.007

Once put into a nondimensional form, the Navier–Stokes equations (A.1), become

$$\begin{aligned}
&\varepsilon^3\left(\partial_T U + U\partial_\xi U + \frac{V\partial_\theta U}{1+\varepsilon\xi} - \frac{V^2}{\varepsilon(1+\varepsilon\xi)}\right)\\
&\quad = -3\varepsilon G\sin\theta - \partial_\xi P + \varepsilon^2\partial_\xi\left(\frac{\partial_\xi[(1+\varepsilon\xi)U]}{1+\varepsilon\xi}\right) + \frac{\varepsilon^4\partial_\theta^2 U}{(1+\varepsilon\xi)^2} - \frac{2\varepsilon^3\partial_\theta V}{(1+\varepsilon\xi)^2},\\
&\varepsilon\left(\partial_T V + U\partial_\xi V + \frac{V\partial_\theta V}{1+\varepsilon\xi} + \frac{\varepsilon UV}{1+\varepsilon\xi}\right)\\
&\quad = -3G\cos\theta - \frac{\partial_\theta P}{1+\varepsilon\xi} + \partial_\xi\left(\frac{\partial_\xi[(1+\varepsilon\xi)V]}{1+\varepsilon\xi}\right) + \frac{\varepsilon^2\partial_\theta^2 V}{(1+\varepsilon\xi)^2} + \frac{2\varepsilon^3\partial_\theta U}{(1+\varepsilon\xi)^2},\\
&\partial_\xi[(1+\varepsilon\xi)U] + \partial_\theta V = 0.
\end{aligned} \tag{A.4}$$

By nondimensionalizing Eqs. (A.3) and (A.4), the boundary conditions on the water–air interface, $\xi = H$, become

$$\begin{aligned}
&-3\mathscr{P}C_p + P - \frac{2\varepsilon^2\partial_\theta H}{N^2(1+\varepsilon H)}\left\{(\varepsilon U + \partial_\theta V)\left[\left(\frac{\varepsilon\partial_\theta H}{1+\varepsilon H}\right)^2 - \frac{1}{\partial_\theta H}\right]\right.\\
&\quad\left. -(1+\varepsilon H)\partial_\xi\left(\frac{V}{1+\varepsilon\xi}\right) - \frac{\varepsilon^2\partial_\theta U}{1+\varepsilon H}\right\}\\
&\quad = \frac{3\overline{S}\varepsilon^3}{N^3}\left[\frac{1}{\varepsilon(1+\varepsilon H)} + 2\frac{\varepsilon(\partial_\theta H)^2}{(1+\varepsilon H)^3} - \frac{\partial_\theta^2 H}{(1+\varepsilon H)^2}\right],\\
&2\mathscr{F}\overline{C}_f - \frac{1}{N^2}\left\{-\frac{4\varepsilon^2\partial_\theta H}{(1+\varepsilon H)^2}(\varepsilon U + \partial_\theta V)\right.\\
&\quad\left. + \left[1 - \left(\frac{\varepsilon\partial_\theta H}{1+\varepsilon H}\right)^2\right]\left((1+\varepsilon H)\partial_\xi\left(\frac{V}{1+\varepsilon\xi}\right) + \frac{\varepsilon^2\partial_\theta U}{1+\varepsilon H}\right)\right\} = 0,\\
&U = \partial_T H + \frac{V\partial_\theta H}{1+\varepsilon H}.
\end{aligned} \tag{A.5}$$

References

Achenbach, E., 1968. Distribution of local pressure and skin friction around a circular cylinder in a cross-flow up to $Re = 5\times10^6$. J. Fluid Mech. 34 (4), 625–639.

Batchelor, G.K., 1994. An Introduction to Fluid Dynamics. Cambridge University Press, Cambridge, p. 64.

Bosdogianni, A., Olivari, D., 1996. Wind- and rain-induced oscillations of cables of stayed bridges. J. Wind Eng. Ind. Aerodyn. 64, 171–185.

Den Hartog, J.P., 1985. Mechanical Vibrations. Dover Publications, Inc., New York, pp. 299–304.

Flamand, O., 1995. Rain–wind-induced vibration of cables. J. Wind Eng. Ind. Aerodyn. 57, 353–362.

Gu, M., Du, X., 2005. Experimental investigation of rain–wind-induced vibration of cables in cable-stayed bridges and its mitigation. J. Wind Eng. Ind. Aerodyn. 93 (1), 79–95.

Hikami, Y., Shiraishi, N., 1988. Rain–wind-induced vibrations of cables in cable-stayed bridges. J. Wind Eng. Ind. Aerodyn. 29, 409–418.

Ibrahim, R.A., 2005. Liquid Sloshing Dynamics. Cambridge University Press, Cambridge, p. 8.

Lemaitre, C., 2006. Dynamique d'un film d'eau sur un hauban de pont soumis au vent. Ph.D. Thesis, Ecole Polytechnique, France.

Please cite this article as: Lemaitre, C., et al., Thin water film around a cable subject to wind, J. Wind Eng. Ind. Aerodyn. (2007), doi:10.1016/j.jweia.2007.02.007

Lemaitre, C., Alam, M., Hémon, P., De Langre, E., Zhou, Y., 2006. Rainwater rivulets on a cable subject to wind. C.-R. Acad. Sci. Méc. 334 (3), 158–163.

Matsumoto, M., Saitoh, T., Kitazawa, M., Shirato, H., Nishizaki, T., 1995. Response characteristics of rain–wind-induced vibration of stay-cables of cable-stayed bridges. J. Wind Eng. Ind. Aerodyn. 57, 323–333.

Oron, A., Davis, S.H., Bankoff, S.G., 1997. Long-scale evolution of thin liquid films. Rev. Mod. Phys. 69 (3), 931–980.

Peil, U., Nahrath, N., 2003. Modeling of rain–wind-induced vibrations. Wind Struct. 6 (1), 41–52.

Peil, U., Nahrath, N., Dreyer, O., 2003. Modeling of rain–wind-induced vibrations. The 11th International Conference on Wind Engineering, Lubbock, Texas, 2003, pp. 389–396.

Reisfeld, B., Bankoff, S.G., 1992. Non-isothermal flow of a liquid film on a horizontal cylinder. J. Fluid Mech. 236, 167–196.

Szechenyi, E., 1975. Supercritical Reynolds number simulation for two-dimensional flow over circular cylinders. J. Fluid Mech. 70 (3), 529–542.

Verwiebe, C., Ruscheweyh, H., 1998. Recent research results concerning the exciting mechanisms of rain–wind-induced vibrations. J. Wind Eng. Ind. Aerodyn. 74–76, 1005–1013.

Wang, Z.J., Zhou, Y., Huang, J.F., Xu, Y.L., 2005. Fluid dynamics around an inclined cylinder with running water rivulets. J. Fluids Struct. 21 (1), 49–64.

Yamaguchi, H., 1990. Analytical study on growth mechanism of rain vibration of cables. J. Wind Eng. Ind. Aerodyn. 33, 73–80.

Please cite this article as: Lemaitre, C., et al., Thin water film around a cable subject to wind, J. Wind Eng. Ind. Aerodyn. (2007), doi:10.1016/j.jweia.2007.02.007